Cohesion and helicity in densely packed dipolar columns

YANYU DUAN[1], ZECHENG GAN[1,2], HO-KEI CHAN[3] and RENÉ MESSINA[4]

[1] *Thrust of Advanced Materials, and Guangzhou Municipal Key Laboratory of Materials Informatics, The Hong Kong University of Science and Technology (Guangzhou), Guangzhou 511453, China*
[2] *Department of Mathematics, The Hong Kong University of Science and Technology, Hong Kong SAR, China*
[3] *School of Science, Harbin Institute of Technology (Shenzhen), Shenzhen 518055, China*
[4] *Université de Lorraine, Laboratoire de Physique et Chimie Théoriques, LPCT - UMR CNRS 7019, 1 Boulevard Arago, 57070 Metz, France*

Abstract – Striking helical structures are known to emerge as dense packings under cylindrical confinement. Yet, their dipolar cohesion upon magnetization remains largely unexplored. Here, we derive analytical relations between chirality, confinement, and cohesion in the nascent helical phase emerging from the densest planar zigzag structure. Excellent agreement with exact chiral lattice-sum calculations is obtained. Remarkably, while the energetic response is harmonic with respect to the chiral distortion, it becomes linear in the experimentally controlled pore diameter. Our results can be realized in confined dipolar assemblies ranging from magnetic colloidal suspensions to granular media.

Introduction. – The self-assembly of dipolar particles under external fields has long served as a paradigmatic model system for understanding collective ordering in soft condensed matter [1–4]. Magnetically aligned colloids confined in cylindrical geometries have been realized experimentally in microtubes [5] and microfluidic devices [6], with applications ranging from magnetic drug delivery [7] and bioimaging [8, 9] to photonic materials [10] and separation technologies [11]. In such systems, long-range dipolar interactions compete with geometrical confinement, giving rise to a rich variety of ordered microstructures.

From a geometrical viewpoint, cylindrical confinement constitutes a remarkable packing problem. As the pore diameter increases, the densest arrangements of identical spheres successively evolve from a single chain to a planar zigzag, a single helix, double helices and increasingly complex columnar structures [12,13]. Over the past two decades, dense packings under cylindrical confinement have provided a fertile ground for exploring structural selection driven solely by geometry [14–26].

Once magnetized, however, these geometrically optimal packings acquire cohesive properties governed by long-range dipolar interactions. While the cohesion of linear dipolar chains and planar zigzag structures has been extensively investigated [27–34], the cohesive properties of the emerging helical branch remain largely unexplored. In particular, the interplay between chirality, confinement, and dipolar cohesion in the vicinity of the zigzag–helix transition has remained elusive.

Recently, we established the cohesive-energy landscape of densely packed confined dipolar columns across the chain–zigzag–helix sequence [35]. While this work provided a first physical picture of the helical regime, a comprehensive analytical description of the nascent helical phase is still missing.

In this Letter, we develop a microscopic analytical theory for the onset of dipolar helicity emerging from the densest planar zigzag packing. Our framework quantitatively captures exact chiral lattice sums and yields remarkably simple relations in terms of either the chiral order parameter or the confinement diameter, thereby elucidating the interplay between geometry, chirality, and dipolar cohesion.

Model. – We consider identical dipolar hard spheres of diameter $d = 1$ confined in a cylindrical pore of diameter D, see Fig. 1. A strong homogeneous magnetic field aligns all dipole moments along the cylinder axis, $\vec{m}_i = m\vec{e}_z$. Using the characteristic dipolar contact energy $U_{\uparrow\uparrow} = \mu_0 m^2/(4\pi)$ as the energy unit, the reduced dipolar interaction between two particles i and j separated by the vector $\vec{r}_{ij} = \vec{r}_j - \vec{r}_i = (x_{ij}, y_{ij}, z_{ij})$ reads

$$v(\vec{r}_{ij}) = \frac{1}{r_{ij}^3}\left[1 - 3\frac{z_{ij}^2}{r_{ij}^2}\right], \tag{1}$$

where $r_{ij} = |\vec{r}_{ij}|$.

We focus on the dense single-helical branch that emerges continuously from the densest planar zigzag configuration upon increasing the pore diameter beyond $D_0 = 1 + \sqrt{3}/2$. The particle positions are parametrized as

$$\vec{r}_n = \left(\frac{a}{2}\cos(n\phi), \frac{a}{2}\sin(n\phi), np\right), \tag{2}$$

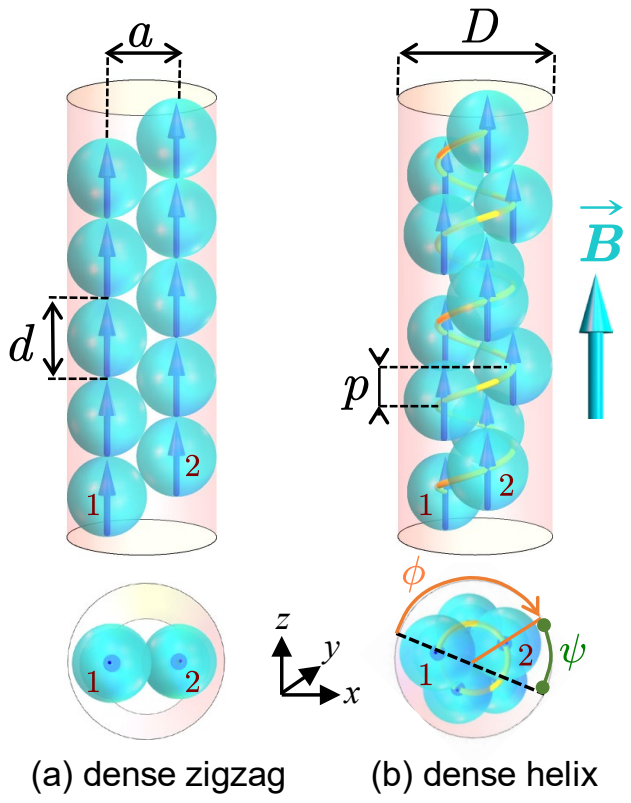

Fig. 1: Geometric setup of dipolar hard spheres with diameter $d = 1$ confined in a cylindrical pore of diameter D and subjected to a strong homogeneous magnetic field $\vec{B} \parallel z$ aligning all dipole moments. (a) Densest planar zigzag configuration at $D_0 = 1 + \sqrt{3}/2$. (b) Dense single-helical branch characterized by the transverse amplitude $a = D - 1$, axial spacing p, and azimuthal phase increment ϕ. The chiral deviation is defined as $\psi = \pi - \phi$, with $\psi = 0$ in the planar zigzag limit.

where

$$a = D - 1 \tag{3}$$

is the diameter accessible to the sphere centers, ϕ is the azimuthal phase increment, and p is the corresponding axial spacing, see also fig. 1.

The dense-packing contact condition yields [25]

$$\phi = \arccos\left(1 - \frac{\sqrt{3}}{a}\right), \qquad p^2 = 1 - \frac{\sqrt{3}}{2}a. \tag{4}$$

and

$$D_0 = 1 + \frac{\sqrt{3}}{2}, \qquad \phi_0 = \pi, \qquad p_0 = \frac{1}{2}, \tag{5}$$

at the zigzag–helix threshold. At this stage, it is natural to introduce the chiral deviation

$$\psi = \pi - \phi. \tag{6}$$

Using $\cos\phi = -\cos\psi$, one obtains

$$a(\psi) = \frac{\sqrt{3}}{1 + \cos\psi}, \tag{7}$$

and

$$p^2(\psi) = 1 - \frac{3}{2(1 + \cos\psi)}. \tag{8}$$

For a particle separated by n sites from the reference particle,

$$r_n^2(\psi) = n^2 p^2(\psi) + \frac{a^2(\psi)}{2}\left[1 - \cos(n\phi)\right]. \tag{9}$$

so that the reduced energy per particle reads

$$u_{\rm helix}(\psi) = \sum_{n=1}^{\infty}\left[\frac{1}{r_n^3} - 3\frac{n^2 p^2(\psi)}{r_n^5}\right]. \tag{10}$$

Near-threshold analysis. – Expanding the helical energy (10) around the densest planar zigzag reference $u_{\rm zz}(D_0)$ naturally yields a Landau expansion in terms of the chiral order parameter ψ,

$$u_{\rm helix}(\psi) - u_{\rm zz}(D_0) = K_2\psi^2 + K_4\psi^4 + \mathcal{O}(\psi^6). \tag{11}$$

The quadratic coefficient naturally separates into even and odd contributions. For even separations,

$$K_2^{\rm even} = \sum_{\substack{n\geq 2\\ n\ \text{even}}} \frac{18}{n^3} = \frac{9}{4}\zeta(3), \tag{12}$$

where $\zeta(s) = \sum_{n=1}^{\infty}\frac{1}{n^s}$ stands for the Riemann zeta function. For odd separations,

$$K_2^{\rm odd} = -18\sum_{\substack{n\geq 1\\ n\ \text{odd}}} \frac{(n^2-3)(3n^2-1)}{(n^2+3)^{7/2}}, \tag{13}$$

and hence

$$K_2 = \frac{9}{4}\zeta(3) - 18\sum_{\substack{n\geq 1\\ n\ \text{odd}}} \frac{(n^2-3)(3n^2-1)}{(n^2+3)^{7/2}}. \tag{14}$$

Introducing the odd Epstein-type lattice function [36],

$$E_{\rm odd}(s;3) = \sum_{\substack{n\geq 1\\ n\ \text{odd}}} \frac{1}{(n^2+3)^s}, \tag{15}$$

one obtains

$$K_2 = \frac{9}{4}\zeta(3) - 18\left[3E_{\rm odd}\left(\frac{3}{2};3\right) - 28E_{\rm odd}\left(\frac{5}{2};3\right) + 60E_{\rm odd}\left(\frac{7}{2};3\right)\right]. \tag{16}$$

Numerically,

$$K_2 \simeq 2.23891217. \tag{17}$$

The fourth-order coefficient is considerably more delicate. After cancellation of the logarithmic divergences arising sepa-

rately in the even and odd contributions, one obtains

$$K_4 = 3\left[\ln 2 + \sum_{\substack{n\geq 1\\ n\ \mathrm{odd}}}\left(\frac{1}{\sqrt{n^2+3}} - \frac{1}{n}\right)\right] + \frac{15}{8}\zeta(3) + \frac{3}{4}\Big[-247E_{\mathrm{odd}}\left(\frac{3}{2};3\right) + 2833E_{\mathrm{odd}}\left(\frac{5}{2};3\right) - 11400E_{\mathrm{odd}}\left(\frac{7}{2};3\right) + 15120E_{\mathrm{odd}}\left(\frac{9}{2};3\right)\Big] \quad (18)$$

Numerically,

$$K_4 \simeq -2.0726931. \quad (19)$$

It is fruitful to rewrite the expansion in terms of the distance to the zigzag–helix threshold

$$\delta = D - D_0, \quad (20)$$

which will be referred to as the excess opening. Exploiting (7),

$$a(\psi) = \frac{\sqrt{3}}{2}\left[1 + \frac{\psi^2}{4} + \frac{\psi^4}{24} + \mathcal{O}(\psi^6)\right], \quad (21)$$

one obtains

$$\delta = \frac{\sqrt{3}}{8}\psi^2 + \frac{\sqrt{3}}{48}\psi^4 + \mathcal{O}(\psi^6), \quad (22)$$

and therefore

$$\psi^2 = \frac{8}{\sqrt{3}}\delta - \frac{32}{9}\delta^2 + \mathcal{O}(\delta^3). \quad (23)$$

Substituting eq. (23) into eq. (11) yields

$$u_{\mathrm{helix}}(D) - u_{\mathrm{zz}}(D_0) = A_1\delta + A_2\delta^2 + \mathcal{O}(\delta^3), \quad (24)$$

with

$$A_1 = \frac{8K_2}{\sqrt{3}}, \quad (25)$$

and

$$A_2 = -\frac{32}{9}K_2 + \frac{64}{3}K_4, \quad (26)$$

noticing that $A_1 > 0$ and $A_2 < 0$.

Discussion. – To assess the accuracy and range of validity of the analytical results derived above, we now compare the near-threshold expansions with the exact lattice-sum predictions. Figure 2 shows the reduced energy difference $\Delta u = u_{\mathrm{helix}}(\psi) - u_{\mathrm{zz}}(D_0)$ as a function of the chiral deviation ψ. Within harmonic theory, the energetic cost of a chiral distortion grows quadratically as $K_2\psi^2$, corresponding to an effective stiffness of the dense helical state near the zigzag–helix threshold. As expected, this approximation accurately captures the initial increase of the energy but progressively overestimates its growth as the distortion amplitude increases.

Crucially, the negative quartic contribution $K_4\psi^4$ softens this harmonic response and substantially improves the agreement with the exact lattice sum, reproducing the curvature of the energy landscape over a broad range of chiral deviations. Remarkably, the quartic approximation remains very accurate well beyond the strict asymptotic regime $\psi \ll 1$ and captures the exact curvature up to chiral deviations approaching $\psi \simeq \pi/4$. This demonstrates that the leading anharmonic correction already captures the essential physics governing the onset of helicity.

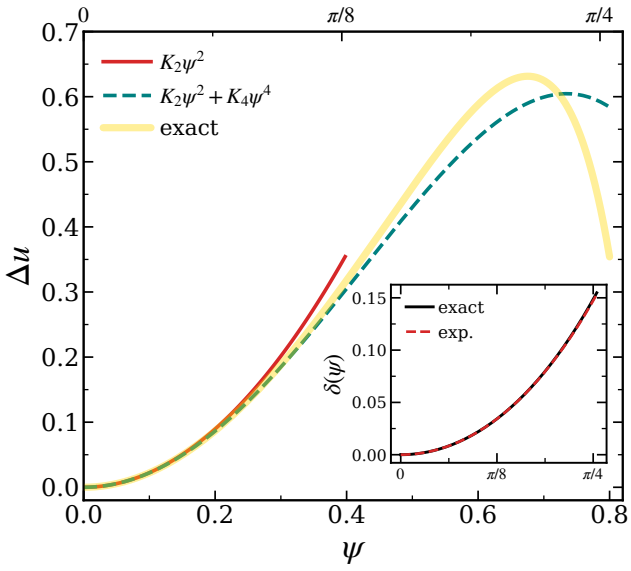

Fig. 2: Reduced energy difference $\Delta u = u_{\mathrm{helix}}(\psi) - u_{\mathrm{zz}}(D_0)$ versus the chiral deviation ψ. Exact lattice sum, eq. (10); eq. (11) truncated at order ψ^2; eq. (11) truncated at order ψ^4. The inset displays $\delta(\psi)$ stemming from the exact geometrical relation, eq. (7), and its near-threshold expansion, see eq. (23).

The inset of fig. 2 further shows that the perturbative relation between the chiral deviation ψ and the excess opening $\delta = D - D_0$ remains extremely accurate over the entire range displayed. The asymptotic expression of $\delta(\psi)$, see eq. (22), is practically indistinguishable from the exact geometrical relation, so that the deviations observed in fig. 2 originate primarily from the energetic expansion itself.

Since the confinement diameter D constitutes the experimentally accessible control parameter, it is natural to reformulate the energetic landscape directly in terms of $\delta = D - D_0$. Thereby, fig. 3 presents the reduced energy difference as a function of the excess opening δ and compares the exact lattice-sum prediction with the expansion provided by eq. (24). As for Fig.2, excellent agreement is observed close to the zigzag–helix threshold. A noteworthy consequence of the geometrical relation $\delta \propto \psi^2$ is that the harmonic energetic response $\Delta u \propto \psi^2$ associated with the chiral order parameter is transformed into a linear dependence on the experimentally controlled quantity, $\Delta u \propto \delta$. Thus, while the onset of helicity is governed by a conventional harmonic energy landscape when expressed in terms of ψ, it no longer appears as a quadratic minimum when viewed as a function of the confinement diameter. This behavior contrasts with the chain–zigzag transition, for which the cohesive energy exhibits the more conventional quadratic dependence on

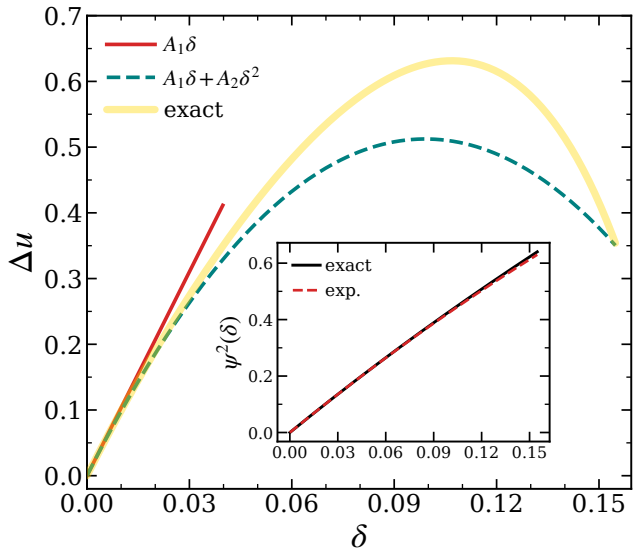

Fig. 3: Reduced energy difference $\Delta u = u_{\rm helix}(D) - u_{\rm zz}(D_0)$ versus the excess opening $\delta = D - D_0$. Exact lattice sum, eq. (10); linear theory, eq. (24) truncated at order δ; quadratic theory, eq. (24) truncated at order δ^2. The inset displays $\psi^2(\delta)$ stemming from the exact geometrical relation, eq. (7), and its near-threshold expansion, eq. (23).

the distance to threshold as recently reported [35].

Moreover, this linear dependence $\Delta u \propto \delta$ also admits a simple mechanical interpretation. Unlike a conventional harmonic energy landscape, for which the restoring force vanishes at the minimum and increases proportionally to the displacement, here we have to deal with a constant force scale at leading order set by A_1. The negative coefficient A_2, on the other hand, reduces this slope as the excess opening increases, giving rise to the downward curvature of the helical branch observed in fig. 3.

All that being said, the first-order approximation correctly captures the initial linear evolution of the cohesive energy but progressively overestimates its growth as the excess opening increases. Remarkably, the inclusion of the second-order term already brings the theory into close agreement with the exact lattice-sum prediction over a broad range of excess openings. Beyond merely improving the quantitative agreement, the negative coefficient A_2 captures the onset of the progressive recovery of cohesion (i.e., decrease of Δu) observed at larger openings, as evidenced by the downward bending of the helical branch, see fig. 3. This indicates that the first nonlinear correction already contains the essential physics governing the post-threshold evolution of the helical state.

Concluding remarks. – To sum up, we have shown that the emergence of helicity in densely packed dipolar columns is governed by a subtle interplay between geometry and long-range dipolar correlations. Starting from the densest planar zigzag configuration, we derived a fully analytical description of the energetic cost associated with the onset of chirality and established explicit connections between the geometrical order parameter, the confinement diameter, and the cohesive energy.

A central result is that the zigzag–helix transition differs qualitatively from the previously studied chain–zigzag transition [35]. While the latter displays the conventional quadratic energetic signature of a structural instability, the zigzag–helix transition appears linear when expressed in terms of the experimentally controlled pore diameter. This unusual behavior provides a simple physical interpretation of the early stages of helix formation and explains how the initially weakened cohesion progressively recovers as the confinement is further relaxed.

These predictions should be directly relevant to experiments on magnetically aligned colloids confined in cylindrical geometries [5] and, more generally, to dipolar assemblies at granular scales [32, 37]. More broadly, the present approach can be extended to other special confinement diameters associated with structural transitions [17, 21] and enhanced cohesion, as well as to *non-circular* cylindrical confinements [38]. This opens new perspectives for understanding how confinement geometry simultaneously controls chirality, structural selection, and cohesion in quasi-one-dimensional dipolar matter.

* * *

Z. G. and Y. D. acknowledge the support from the Natural Science Foundation of China (Grant No. 12201146); and Guangzhou-HKUST(GZ) joint research project (Grant No. 2023A03J0003 and 2024A03J0606). H. K. C. would like to acknowledge financial support from the Guangdong Basic and Applied Basic Research Foundation, China (Grant No. 2024A1515011585).

REFERENCES

[1] LÖWEN H., *J. Phys. Condens. Matter*, **13** (2001) R415.
[2] HOLM C. and WEIS J.-J., *Curr. Opin. Colloid Interface Sci.*, **10** (2005) 133.
[3] FARAUDO J., ANDREU J. S. and CAMACHO J., *Soft Matter*, **9** (2013) 6654.
[4] IVANOV A. O. and ZUBAREV A., *Materials*, **13** (2020) 3956.
[5] LIU P., DE FOLTER J. W. J., PETUKHOV A. V. and PHILIPSE A. P., *Soft Matter*, **11** (2015) 6201.
[6] LACHARME F., VANDEVYVER C. and GIJS M. A. M., *Microfluid. Nanofluid.*, **7** (2009) 479.
[7] DURÁN J., ARIAS J., GALLARDO V. and DELGADO A., *J. Pharm. Sci.*, **97** (2008) 2948.
[8] FREY N. A., PENG S., CHENG K. and SUN S., *Chem. Soc. Rev.*, **38** (2009) 2532.
[9] DAS G. K., ZHANG Y., D'SILVA L., PADMANABHAN P., HENG B. C., CHYE LOO J. S., SELVAN S. T., BHAKOO K. K. and YANG TAN T. T., *Chem. Mater.*, **23** (2011) 2439.
[10] LIU T., CHAN H.-K. and WAN D., *Soft Matter*, **19** (2023) 7313.
[11] HAN H., JOHNSON A., KACZOR J., KAUR M., PASZCZYNSKI A. and QIANG Y., *J. Appl. Phys.*, **107** (2010) .
[12] PICKETT G. T., GROSS M. and OKUYAMA H., *Phys. Rev. Lett.*, **85** (2000) 3652.
[13] WINKELMANN J. and CHAN H.-K., *Columnar structures of spheres: Fundamentals and applications* (Jenny Stanford Publishing, Singapore) 2023.
[14] CHAN H.-K., *Phys. Rev. E*, **84** (2011) 050302.

[15] CHAN H.-K., *Philos. Mag.*, **93** (2013) 4057.
[16] DURÁN-OLIVENCIA F. and GORDILLO M., *Phys. Rev. E*, **79** (2009) 061111.
[17] FU L., STEINHARDT W., ZHAO H., SOCOLAR J. E. and CHARBONNEAU P., *Soft Matter*, **12** (2016) 2505.
[18] FU L., BIAN C., SHIELDS C. W., CRUZ D. F., LÓPEZ G. P. and CHARBONNEAU P., *Soft Matter*, **13** (2017) 3296.
[19] KOGA K. and TANAKA H., *J. Chem. Phys.*, **124** (2006) 131103.
[20] LOHR M. A., ALSAYED A. M., CHEN B. G., ZHANG Z., KAMIEN R. D. and YODH A. G., *Phys. Rev. E*, **81** (2010) 040401.
[21] MUGHAL A., CHAN H. K. and WEAIRE D., *Phys. Rev. Lett.*, **106** (2011) 115704.
[22] MUGHAL A., CHAN H., WEAIRE D. and HUTZLER S., *Phys. Rev. E*, **85** (2012) 051305.
[23] MUGHAL A., *Philos. Mag.*, **93** (2013) 4070.
[24] YAMCHI M. Z. and BOWLES R. K., *Phys. Rev. Lett.*, **115** (2015) 025702.
[25] CHAN H.-K., WANG Y. and HAN H., *AIP Adv.*, **9** (2019) 125118.
[26] MUGHAL A. and WEAIRE D., *Phys. Rev. E*, **89** (2014) 042307.
[27] HALSEY T. C. and TOOR W., *Journal of Statistical Physics*, **61** (1990) 1257.
[28] TAO R. and SUN J. M., *Phys. Rev. Lett.*, **67** (1991) 398.
[29] FARAUDO J. and CAMACHO J., *Colloid Polym. Sci.*, **288** (2010) 207.
[30] DARRAS A., FISCINA J., PAKPOUR M., VANDEWALLE N. and LUMAY G., *Eur. Phys. J. E*, **39** (2016) 47.
[31] MESSINA R. and SPITERI L., *Eur. Phys. J. E*, **39** (2016) 81.
[32] MESSINA R. and STANKOVIĆ I., *Physica A*, **466** (2017) 10.
[33] KEMGANG E. and MESSINA R., *Phys. Rev. E*, **105** (2022) L012602.
[34] MESSINA R. and KEMGANG E., *J. Chem. Phys.*, **159** (2023) .
[35] DUAN Y., GAN Z., MOHRBACH H., CHAN H.-K. and MESSINA R., *J. Chem. Phys.*, **164** (2026) 064905.
[36] EPSTEIN P., *Math. Ann.*, **56** (1903) 615.
[37] VANDEWALLE N. and DORBOLO S., *New J. Phys.*, **16** (2014) 013050.
[38] WANG X., GUO J. and LI Y., *Nature Comm.*, (2026) in press.